Evolution of Void Shape and Size in Creeping Solids

Needleman, Alan; Tvergaard, Viggo; Giessen, Erik van der

Published in:
International Journal of Damage Mechanics

DOI:
10.1177/105678959500400203

Evolution of Void Shape and Size in Creeping Solids

ALAN NEEDLEMAN*
Division of Engineering
Brown University
Providence, RI 02912

VIGGO TVERGAARD
Department of Solid Mechanics
Technical University of Denmark
Lyngby, Denmark

ERIK VAN DER GIESSEN
Laboratory for Engineering Mechanics
Delft University of Technology
Delft, The Netherlands

ABSTRACT: A boundary value problem for a periodic array of initially spherical voids in a power law creeping solid is analyzed. An axisymmetric cell model relevant for simulating grain boundary void growth is used. The rate boundary value problem is solved by means of a finite element method. Void growth histories accounting for void shape changes and, within the cell model context, void interaction effects are computed for various remote stress triaxiality states. An automatic remeshing algorithm permits computations for large changes in void size and shape. The computed void growth rates are compared with predictions from available analytical formulas that neglect shape change effects.

INTRODUCTION

THE GROWTH OF small voids in inelastic solids plays an important role both in studies of ductile fracture of metals at room temperature and in studies of creep rupture at elevated temperatures. Investigations of the full failure process involve the nucleation of voids, which tends to occur at second phase particles,

*Author to whom correspondence should be addressed.

1056-7895/95/02 0134-19 $10.00/0

and the growth of voids toward coalescence with neighboring voids. In the early stage of void growth, when the void volume fraction is still very low, the interaction with neighboring voids is negligible; but interaction plays an increasing role as the void volume fraction grows and is completely dominant in the final stages of coalescence. Many investigations have focused on different aspects of the effect of void growth on material failure, see for example the reviews of Tvergaard (1990) and Needleman, Tvergaard and Hutchinson (1992). Compared to the earlier model of material damage proposed by Kachanov (1986), these investigations of void growth can be regarded as detailed micromechanical studies for a particular type of failure mechanism.

For a void growing in a viscous material under remote axisymmetric loading, Budiansky, Hutchinson and Slutsky (1982) have made a detailed study of the evolution of void volume and shape as a function of time and remote stress state. It has been found by Eshelby (1957) that an isolated ellipsoidal void in an infinite, linearly viscous solid under uniform stress will remain ellipsoidal. This has been used by Budiansky et al. (1982) to determine the asymptotic shapes of initially spherical voids for all combinations of axisymmetric stress components. For compressive stresses, the voids can collapse into a penny-shaped crack, a needle or a point, whereas for tensile stress states, the void volume grows toward infinity with asymptotic shapes that are either oblate or prolate spheroids, cylinders or needles. Similar results for a material undergoing nonlinear creep require a full numerical analysis. Budiansky and Hutchinson (1980) have studied a void in a power law creeping material and have determined self-similar void shapes for a wide range of creep exponents and stress states. Thus, they have identified regimes where the asymptotic shapes are either oblate or prolate pseudo-spheroids, or cylinders. Lee and Mear (1994) have gone a step further to determine the shape development during growth in a power law creeping material. A common feature of these analyses for void growth in viscous materials is that only a single void in an infinite solid is considered, so that any effect of interaction with neighboring voids is neglected.

The present paper considers void growth in a power law creeping material containing a periodic array of initially spherical voids. Assuming an axisymmetric stress state in the material, the void growth behavior is reasonably well represented in terms of an axisymmetric unit cell model analysis (e.g., see Needleman and Rice, 1980; Tvergaard, 1982). The cell model used here is that used by Needleman and Rice (1980), Sham and Needleman (1983) and Van der Giessen et al. (1995) to analyze the growth of grain boundary cavities by the combined effects of power law creep and grain boundary diffusion. In those studies, the instantaneous rate of change of the void volume was determined. Here, attention is confined to power law creep, but the effect of void interaction and void shape change on the void growth rate is analyzed for large increases of the void volume compared to the initial value.

MODEL FORMULATION AND METHOD OF SOLUTION

We consider a porous creeping solid in which the voids are arranged primarily in parallel sheets of doubly periodic arrays of voids. The spacing between such void sheets is assumed to be large enough compared to the mean spacing in the plane of the sheets so that the interaction between voids in different sheets can be neglected, but the interactions between voids within a sheet are accounted for approximately. We assume that in the initial undeformed state, the voids are spherical with average radius a_0 and have a mean planar spacing of $2b_0$ (see Figure 1). In the course of the deformation process, the voids will grow and change in shape, and also the void spacing $2b$ will change. The deformations are modelled by an axisymmetric cell analysis using a cylindrical unit cell perpendicular to the grain boundary which has an initial diameter $2b_0$ and height $2h_0$, and the void at its center. Because of symmetry, only half of the cell needs to be considered as shown in Figure 2. Consistent with this axisymmetric model, we consider the remote stress system to be axially symmetric with respect to the axis of the cylinder. Employing a cylindrical coordinate system (r, ϕ, z) with the z-axis aligned with the axis of symmetry, the nonvanishing remote stresses σ_{ij}^{∞} are

$$\sigma_{rr}^{\infty} = T \qquad \sigma_{zz}^{\infty} = S \tag{1}$$

Throughout this work, we shall take $S > T > 0$.

The matrix material is modelled as being incompressible and to deform purely by power law creep, governed by the following constitutive relation:

$$\dot{\epsilon}_{ij} = \dot{\epsilon}_e \frac{3}{2} \frac{s_{ij}}{\sigma_e} \qquad \dot{\epsilon}_e = \dot{\epsilon}_0 \left(\frac{\sigma_e}{\sigma_0} \right)^n \tag{2}$$

where $\dot{\epsilon}_{ij}$ and s_{ij} are the strain-rate and stress-deviator components, respectively, in the current configuration. Here, n is the creep exponent, $\dot{\epsilon}_0$ and σ_0 are reference strain-rate and stress quantities for the material, while $\dot{\epsilon}_e = \sqrt{2\dot{\epsilon}_{ij}\dot{\epsilon}_{ij}/3}$ and $\sigma_e = \sqrt{3s_{ij}s_{ij}/2}$ are the effective strain-rate and Mises effective stress, respectively. Remote from the voids, the effective and mean stresses are given by

$$\sigma_e^{\infty} = S - T \equiv \sigma_{\infty} \qquad \sigma_m^{\infty} = \frac{1}{3}(S + 2T) \tag{3}$$

respectively, and the corresponding strain-rate components for an infinite medium are

$$\dot{\epsilon}_{zz}^{\infty} = -2\dot{\epsilon}_{rr}^{\infty} = -2\dot{\epsilon}_{\phi\phi}^{\infty} = \dot{\epsilon}_{\infty} \tag{4}$$

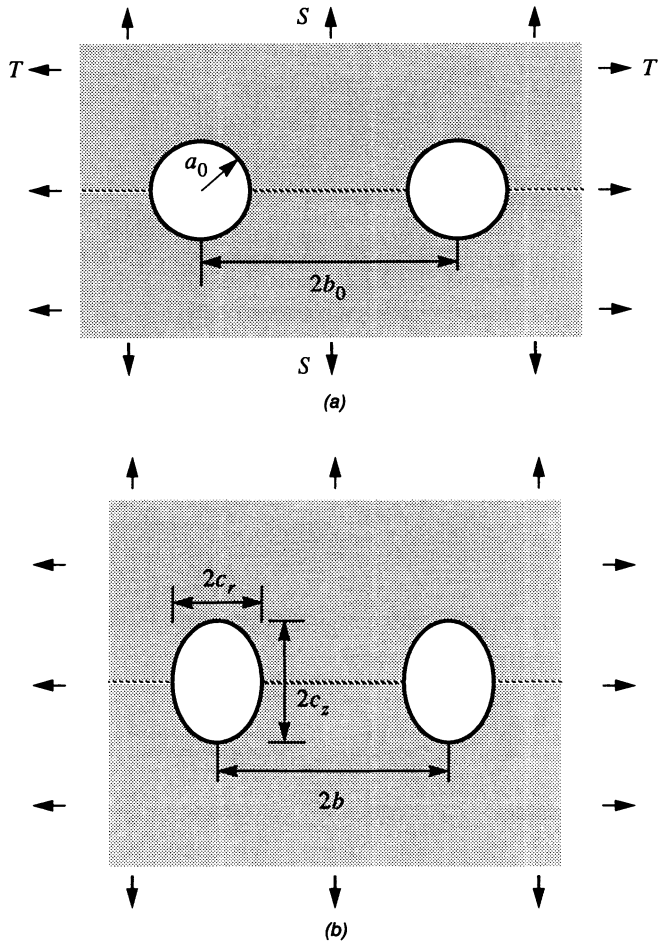

Figure 1. *A void sheet in a creeping solid subjected to constant remote axial stressing* S, T. *(a) initial state, (b) current state.*

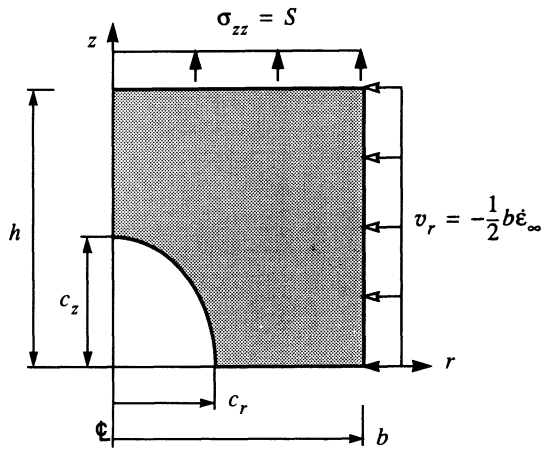

Figure 2. *Half of the unit cell used in the analysis. Periodic boundary conditions are prescribed on the lateral surface of the cylinder, while the remote axial stress is prescribed on the faces of the cell.*

where $\dot{\epsilon}_\infty$ is the remote effective strain-rate,

$$\dot{\epsilon}_\infty = \dot{\epsilon}_0 \left(\frac{\sigma_\infty}{\sigma_0}\right)^n \tag{5}$$

The boundary conditions for the cell problem are taken as follows:

$$v_r = b\dot{\epsilon}_{rr}^\infty \quad \sigma_{rz} = 0 \quad \text{along } r = b \tag{6}$$

$$v_z = 0 \quad \sigma_{rz} = 0 \quad \text{along } z = 0 \tag{7}$$

$$\sigma_{zz} = S \quad \sigma_{rz} = 0 \quad \text{along } z = h \tag{8}$$

The kinematic boundary condition in Equation (6) ensures that the unit cell represents the periodic array of voids as shown in Figure 1, by prescribing the lateral surface of the cylinder to remain straight. The current radius of the cylinder is denoted by b. The boundary condition (8) is used to simulate creep under remote axial stress. As a consequence, the end surface of the cylinder, $z = h$, is not constrained to remained flat. Enforcing this constraint, in conjunction with constant remote stress, would significantly complicate the numerical procedure. With Equation (8), variations in the current height of the cylinder, h, will remain negligible as long as the initial height h_0 is large enough.

The problem under consideration can be conveniently formulated through a

minimum principle stated by Hill (1956). With reference to the current deformed state, the variational principle states that $\delta F(v_i) = 0$, with

$$\frac{1}{4\pi} F(v_i) = \frac{n}{1+n} \sigma_0 \dot{\epsilon}_0 \int_0^h \int_{r_0(z)}^b \left(\frac{\dot{\epsilon}_e}{\dot{\epsilon}_0}\right)^{(1+n)/n} r dr dz - S \int_0^b r v_z(r,h) dr \qquad (9)$$

for all kinematically admissible velocity fields $v_i(r,z)$; that is, for velocities that satisfy the kinematic boundary conditions in Equations (6)–(7) and that are isochoric,

$$\dot{\epsilon}_{kk} = v_{k,k} = 0 \qquad (10)$$

The function $r_0(z)$ in Equation (9) is the current cavity radius at height z, if z is within the current cavity height and is zero otherwise.

The numerical solution to the variational problem [Equations (9–10)] is obtained through the finite element formulation of Needleman and Shih (1978). This particular technique is characterized by the fact that the incompressibility constraint Equation (10) is imposed directly by making use of "super-elements" built up of quadrilateral elements. The quadrilaterals in turn comprise four triangular elements in a "crossed triangle" configuration. The discretized nonlinear equations are solved by a Newton-Raphson iterative procedure, with under-relaxation used to facilitate convergence.

The finite strain evolution of the void is computed in a linear incremental fashion. At the end of a time step, the position of a nodal point, $\mathbf{x}$, is given by $\mathbf{x}(t + \Delta t) = \mathbf{x}(t) + \mathbf{v}(t)\Delta t$. The new void shape is then known from the positions of the nodal points along the void surface. Similarly, the new value of the cell radius is known from the position of the nodal points along $r = b$. The cell is required to stay a circular cylinder, and the updated cell height is computed by averaging the updated nodal positions along $z = h$. With $a_0/h_0 = 0.1$ and with the time steps used, the variation in the updated z-coordinates along $z = h$ was typically in the fourth significant figure. Once the new cell height was identified, the finite element mesh was re-designed automatically, on the basis of the current shapes of the cylindrical cell and the void. It is worth noting that because the material is purely viscous, the mechanical response is history independent and no field quantities need to be transferred from the old mesh to the new mesh.

In a given configuration, the present model problem is similar to that for coupled diffusive and creep growth of grain boundary cavities used by Needleman and Rice (1980), Sham and Needleman (1983) and very recently by Van der Giessen et al. (1995), but represents the limiting case that diffusive transport of matter is negligible. However, these studies confined attention to the instantaneous rate of change of the void volume, and did not study the temporal evolu-

tion of the void shape. The void evolution study by Lee and Mear (1994) on the other hand, is for voids in infinite creeping media and thus, neglects void interaction effects. It should be noted (see also Van der Giessen et al., 1995) that, because of the kinematic boundary condition in Equation (6), the present model primarily incorporates the interaction among voids that are periodically spaced on a plane. This relates directly, for instance, to grain boundary cavities, but the more uniform spatial void-void interaction in a homogeneously porous solid is not necessarily well represented by the present cell model.

RESULTS

Calculations are carried out for $a_0/b_0 = 0.1$, $a_0/h_0 = 0.1$ and for $T/S = 0.75$, 0.6 and 0, which correspond to remote stress triaxialities, $\sigma_m^\infty/\sigma_\infty$, of 3.333, 1.833 and 0.333, respectively. The creep exponent is specified as $n = 5$, which is a representative value for structural metals deforming by dislocation creep, and a few comparisons are made with results for $n = 1$.

Figure 3 shows the initial finite element mesh and the final meshes generated by the automatic remeshing procedure for $n = 5$ with three values of T/S. The initial mesh consists of sixteen uniformly spaced quadrilateral elements around the surface of the void and twenty-two quadrilateral elements of graduated size between the void surface and the cell boundary. At each time step, a new spacing of the nodal points on the void surface is generated so that the interval-to-interval variation falls within a specified tolerance. The first eight points on the void surface connect to eight uniformly spaced points along $r = b$, while the last eight points connect to eight uniformly spaced points on $z = h$. The dividing point (there are seventeen nodal points on the void surface) connects to the cell corner $r = b, z = h$. The gradation between the void surface and the cell boundary follows the same proportions as in the original mesh. In the calculations here, the new mesh has the same number of nodal points as the mesh it replaces, although the remeshing algorithm can accommodate a different number of nodal points in the old and new meshes. It is important to note that during remeshing, the nodal points do not move with material points so that the mesh spacings in Figure 3 do not reflect the strain distribution. Substantial void growth and change in void shape can be seen in Figure 3. Defining the intersection of the void surface with the r-axis by c_r and the intersection with the z-axis by c_z [see Figures 1(b) and 2]; $c_r/a_0 = 0.68$ and $c_z/a_0 = 2.8$ for $T/S = 0$ [Figure 3(b)]; $c_r/a_0 = 3.6$ and $c_z/a_0 = 3.9$ for $T/S = 0.6$ [Figure 3(c)]; and $c_r/a_0 = 3.9$ and $c_z/a_0 = 3.3$ for $T/S = 0.75$ [Figure 3(d)].

Curves of void growth rate and aspect ratio, c_r/c_z, versus strain for these three calculations are shown in Figure 4. Here, ϵ_∞ is identified with $-2 \ln (b/b_0)$; see Equations (4) and (6). In Figure 4(a), the void growth rate, $\dot{V}$, is normalized by the remote strain rate, $\dot{\epsilon}_\infty$, and by a_0^3, where a_0 is the initial void radius. Also,

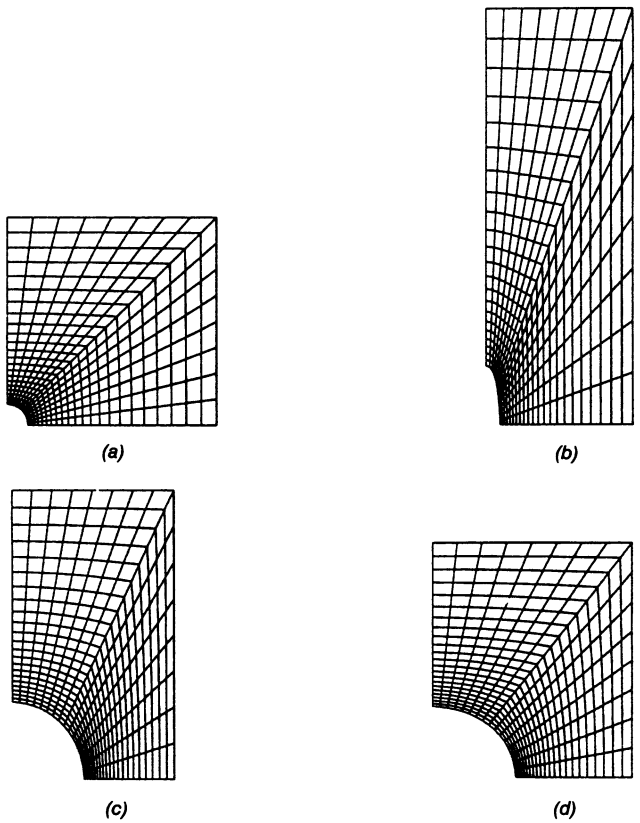

Figure 3. *(a) Initial finite element mesh; (b) finite element mesh for* T/S = *0,* n = *5 at* ϵ_∞ = *0.69; (c) finite element mesh for* T/S = *0.6,* n = *5 at* ϵ_∞ = *0.37; (d) finite element mesh for* T/S = *0.75,* n = *5 at* ϵ_∞ = *0.083. Each quadrilateral consists of four "crossed" triangles.*

because of the wide range in void growth rates, a log scale is used where log denotes the base 10 logarithm. With $T/S = 0.75$, the void growth rate increases by a factor of about 200 between $\epsilon_\infty = 0$ and $\epsilon_\infty = 0.083$; with $T/S = 0.6$, the increase in void growth rate is substantially slower, varying by about a factor of 100 between $\epsilon_\infty = 0$ and $\epsilon_\infty = 0.37$. With $T/S = 0$, the void growth rate decreases with increasing strain and is about 1/7 its initial value at $\epsilon_\infty = 0.69$. The mesh plots in Figure 3 correspond to the end points on the void growth curves in Figure 4(a).

The aspect ratio curves in Figure 4(b) provide an indication of when void interaction effects become significant. With $T/S = 0.75$ and $n = 5$, the asymptotic shape for an isolated spherical void is an oblate spheroid ($c_r/c_z > 1$) with

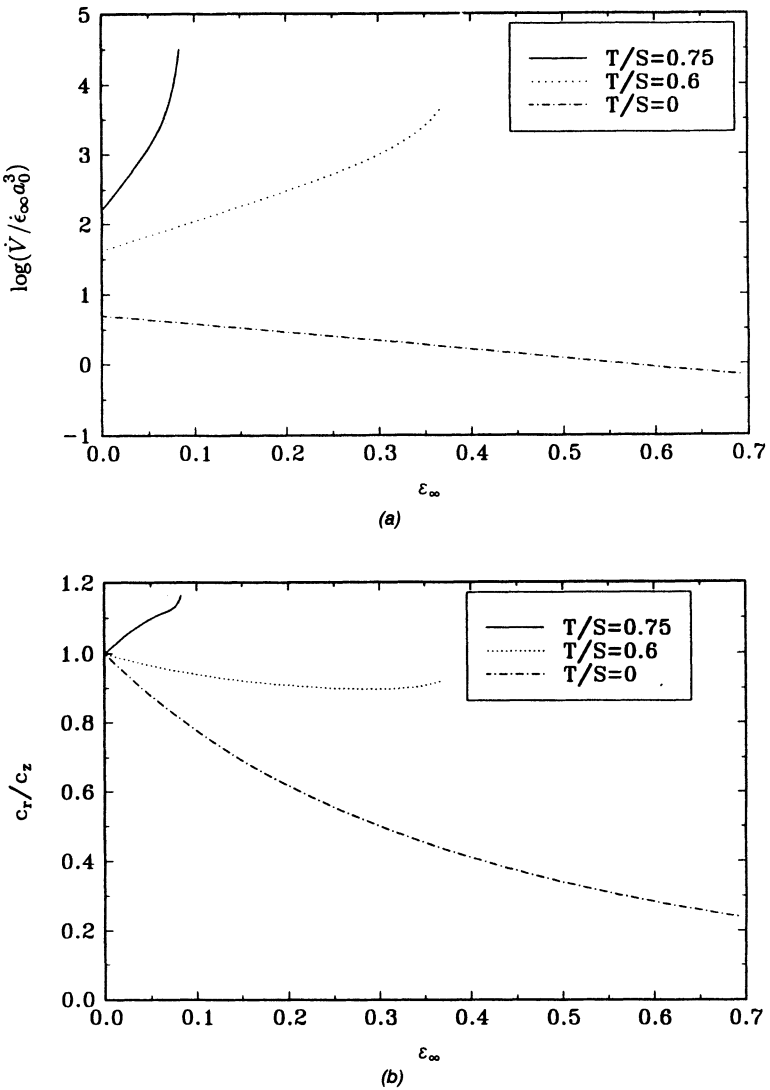

Figure 4. *Curves of normalized void growth rate versus remote strain with* $n = 5$ *and* $a_0/b_0 = 0.1$.

$c_r/c_z \approx 1.2$, Budiansky and Hutchinson (1980). The initial tendency toward an oblate spheroid is seen in Figure 4(b) for $T/S = 0.75$. The slope of the aspect ratio versus strain curve at first decreases with increasing deformation, then after some growth, there is a rapid increase in aspect ratio due to void interaction effects. On the other hand, with $T/S = 0.6$, Budiansky and Hutchinson (1980) have shown that an isolated spherical void tends to become slightly prolate ($c_r/c_z \approx 0.9$). In Figure 4(b), for $T/S = 0.6$, the aspect ratio c_r/c_z indeed reaches a minimum value of 0.90 at $\epsilon_\infty = 0.28$ and then increases due to necking down between the voids. With $T/S = 0$, c_r/c_z is still decreasing noticeably at $\epsilon_\infty = 0.69$.

The amount of void growth can be obtained by integrating the void growth curves in Figure 4(a). The ratio of final void volume to initial void volume, V/V_0, is 49.3 for $T/S = 0.75$, 49.2 for $T/S = 0.6$ and 1.37 for $T/S = 0$. The void volume can also be estimated by assuming that the void shape is a spheroid with axes c_r and c_z. Using the values of c_r and c_z in Figure 3, the void volume ratios so estimated are 50.9, 50.3 and 1.30 for $T/S = 0.75$, 0.6 and 0, respectively. This suggests that the void shapes in Figure 3 do not differ substantially from a spheroid.

To give an indication of the computational effort involved, the calculations with $n = 5$ took from 14 s ($T/S = 0$) to 32 s ($T/S = 0.75$) per time step (the CPU time per time step depends on the number of Newton-Raphson iterations) on a DEC Alpha 3000/500 workstation. Thirty time steps were used with $T/S = 0.75$ and one hundred time steps with $T/S = 0$, so that the total time for a computation varied between sixteen and twenty-four minutes. The time step was specified by setting the absolute value of the largest component of $\mathbf{v}\Delta t$ to $0.1a_0$. The calculation with $T/S = 0.75$ was repeated with the maximum displacement reduced to $0.05\ a_0$ and the void growth rate curve obtained was indistinguishable from the corresponding curve in Figure 4(a).

Contours of mean normal stress, σ_m, normalized by the remote effective stress, σ_∞, are plotted in Figure 5 for the calculation with $T/S = 0.75$ at $\epsilon_\infty = 0.075$ and at the last stage of deformation computed, $\epsilon_\infty = 0.083$. At $\epsilon_\infty = 0.075$, $V/V_0 = 22.8$. The development of the hydrostatic tension peak near $r = b$, $z = 0$, is an indication of the interaction between neighboring voids. The corresponding effective strain rate contours, $\dot{\epsilon}_e/\dot{\epsilon}_\infty$, in Figure 6 show the intensification in the strain rate concentration along the void surface near the r-axis. In Figure 6(b), the effective strain rate is more than an order of magnitude greater than the remote strain rate all along the ligament between adjacent voids. At $\epsilon_\infty = 0.083$, the stress and strain rate distributions are consistent with a deformation mode that involves the necking down of the ligament between neighboring voids. For nearly rate independent solids, Koplik and Needleman (1988) found a rather abrupt transition to the necking down mode of deformation. For the highly viscous creeping solid considered here, the transition is more gradual. Also note

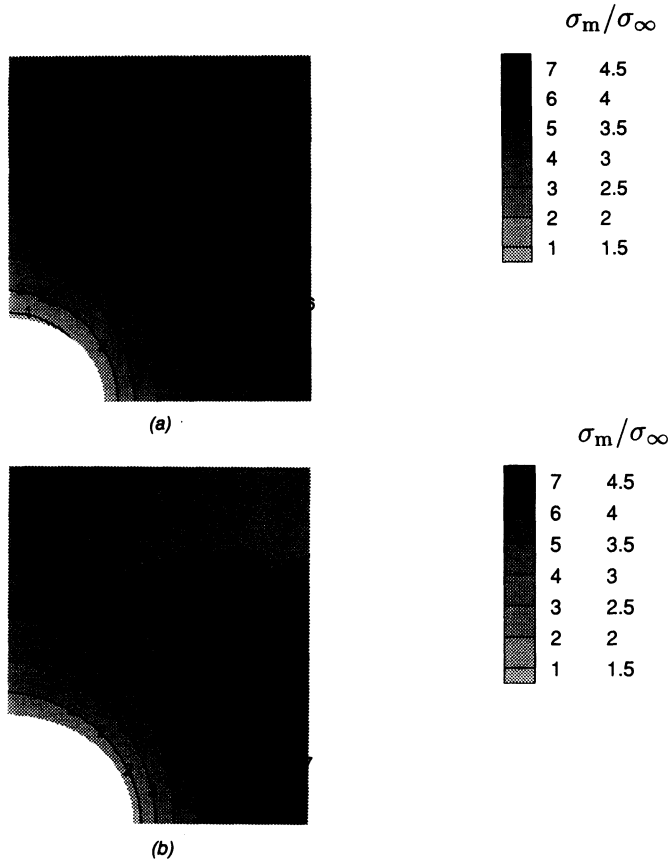

Figure 5. *Contours of σ_m/σ_∞ with* n = 5, $a_0/b_0 = 0.1$ *and* T/S = 0.75 *at (a)* $\epsilon_\infty = 0.075$; *(b)* $\epsilon_\infty = 0.083$.

that although the strain rate distribution in Figure 6 is rather nonhomogeneous along $z = h$, the strain rates are so small there (relative to the maximum strain rate) that the resulting nonuniformity in the displacements along $z = h$ is small.

Figures 7 and 8 show contour plots of normalized mean normal stress, σ_m/σ_∞, and normalized effective strain rate, $\dot{\epsilon}_e/\dot{\epsilon}_\infty$, for $T/S = 0.6$ at $\epsilon_\infty = 0.37$ and for $T/S = 0$ at $\epsilon_\infty = 0.69$, respectively. The hydrostatic tension has a peak at the center of the ligament between adjacent voids in Figure 7(a), which indicates that void interactions are coming into play. In Figure 7, $V/V_0 = 49.2$ so that comparing these field distributions with those in Figures 5(b) and 6(b), where $V/V_0 = 49.3$, shows the effect of stress triaxiality at essentially the same stage of void growth. With $T/S = 0.6$, the high strain rates are confined to a smaller re-

gion, and the strain rate concentration is more focused at the point where the void surface intersects the r-axis. The hydrostatic tension exhibits a similar concentration at the midpoint of the ligament between adjacent voids. In Figure 8, where $T/S = 0$, the fields are essentially uniform except very near the void. For both $T/S = 0.6$ [Figure 7(b)] and $T/S = 0$ [Figure 8(b)], the strain rate distribution is rather uniform along $z = h$.

In Figure 9, the void volume growth rates obtained for the nonlinear viscous solid with $n = 5$ are compared on a log scale with those predicted based on a linear viscous relation, $n = 1$, for the same remote values of $\dot{\epsilon}_\infty$, considering the cases $T/S = 0.6$ and $T/S = 0$. With $T/S = 0.6$, the void volume growth rate is much larger with $n = 5$ than with $n = 1$. For example, at $\epsilon_\infty = 0.31$,

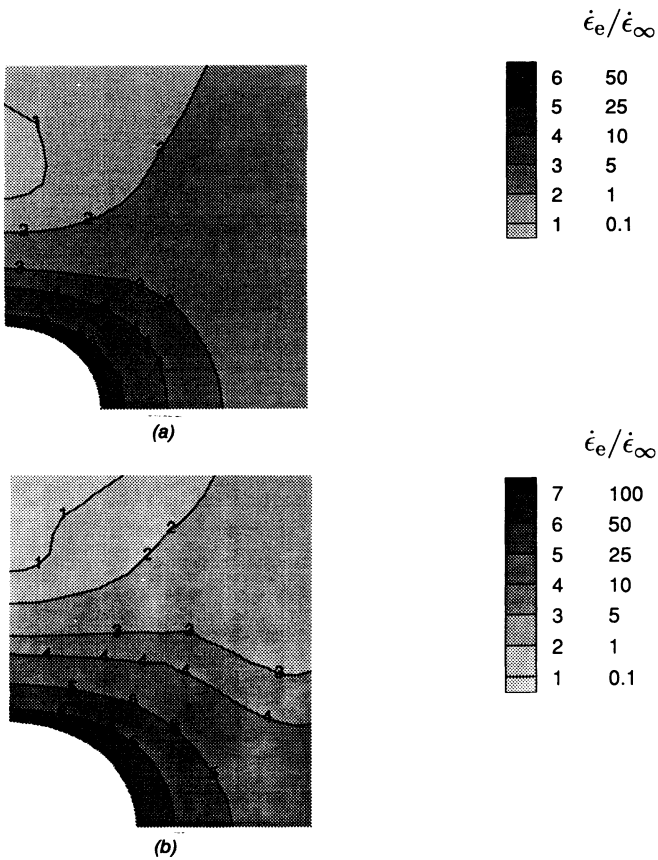

Figure 6. *Contours of* $\dot{\epsilon}_e/\dot{\epsilon}_\infty$ *with* n = 5, $a_0/b_0 = 0.1$ *and* T/S = 0.75 *at (a)* $\epsilon_\infty = 0.075$; *(b)* $\epsilon_\infty = 0.083$.

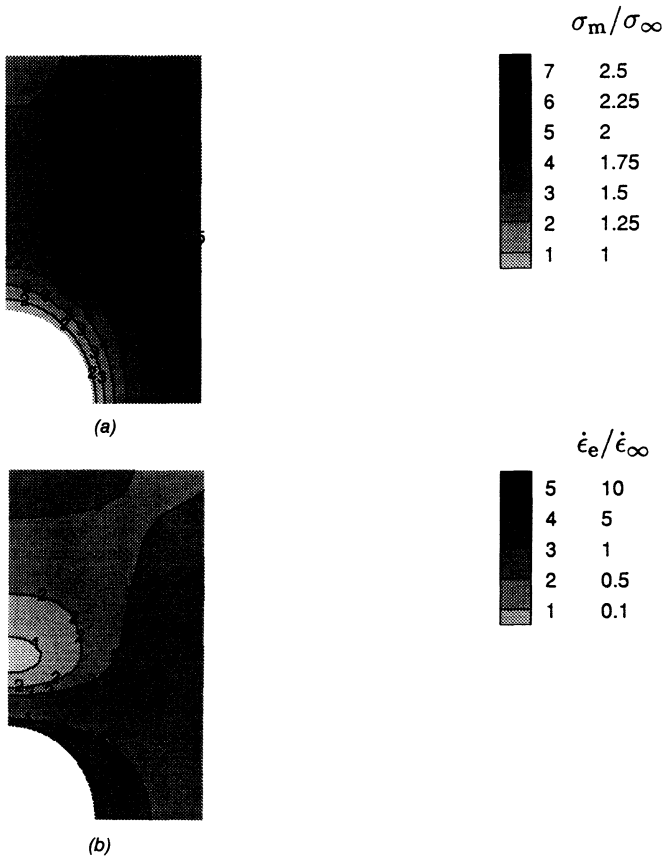

Figure 7. *Contours of (a)* σ_m/σ_∞ *and (b)* $\dot{\epsilon}_e/\dot{\epsilon}_\infty$ *with* n = 5, $a_0/b_0 = 0.1$ *and* T/S = 0.6 *at* $\epsilon_\infty = 0.37$.

$\dot{V}(n = 5)/\dot{V}(n = 1) = 22$. On the other hand, with $T/S = 0$, the void volume growth rate is not very sensitive to the value of n. Initially, at $\epsilon_\infty = 0$, $\dot{V}(n = 5)/\dot{V}(n = 1) = 1.60$, while at $\epsilon_\infty = 0.69$, $\dot{V}(n = 5)/\dot{V}(n = 1) = 1.24$. For an isolated spherical void embedded in a linear creeping solid, the initial void volume growth rate is $\dot{V}/(\dot{\epsilon}_\infty a_0^3) = \pi$ and, asymptotically, $V/V_0 = 1.26$, Budiansky and Hutchinson (1980), Budiansky et al. (1982). The numerical results using the mesh in Figure 3(a) give an initial void volume growth rate of $\dot{V}/(\dot{\epsilon}_\infty a_0^3) = 3.08$ and $V/V_0 = 1.24$ at $\epsilon_\infty = 0.69$. At $\epsilon_\infty = 0.69$, V/V_0 is increasing, but very slowly. At least in this case, the discretization in Figure 3(a) reproduces the analytical results to within about 2% accuracy.

Accurate analytical expressions for the void volume growth rate are of use, for

instance, in developing theories of creep rupture. Figure 10 shows a comparison between the numerically predicted void growth rates and those given by two sets of analytical expressions. One is the expression of Budiansky et al. (1982), obtained for a spherical void of a power law creeping material embedded in an infinite medium for high, positive triaxialities $\sigma_m^\infty/\sigma_\infty$,

$$\frac{\dot{V}}{\dot{\epsilon}_\infty V} = \frac{3}{2}\left\{\alpha_n\left(\frac{\sigma_m^\infty}{\sigma_\infty}\right) + \beta_n\right\}^n \tag{11}$$

where

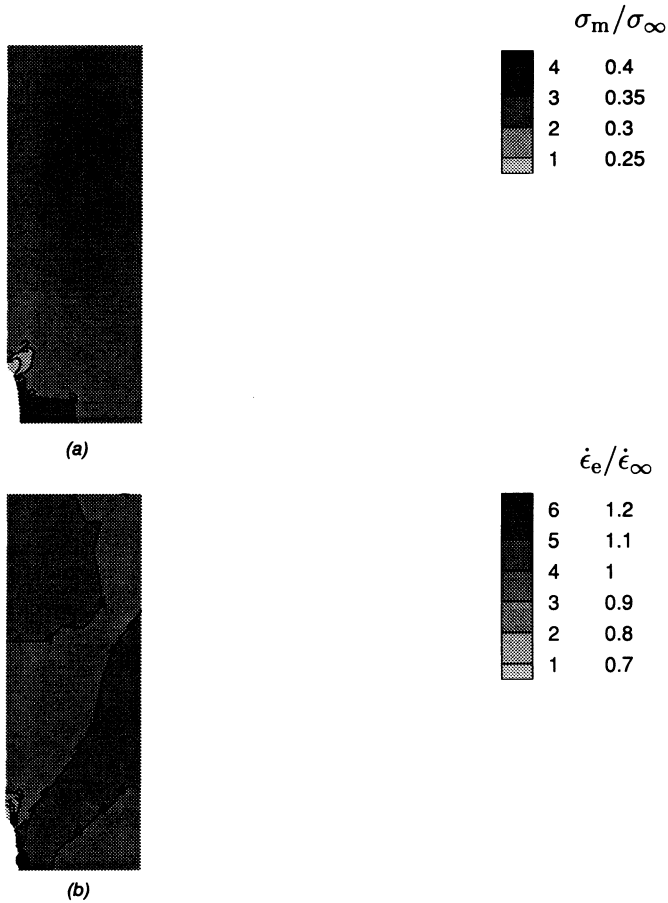

Figure 8. *Contours of (a)* σ_m/σ_∞ *and (b)* $\dot{\epsilon}_e/\dot{\epsilon}_\infty$ *with* n = 5, $a_0/b_0 = 0.1$ *and* T/S = 0 *at* $\epsilon_\infty = 0.69$.

$$\alpha_n = \frac{3}{2n} \qquad \beta_n = \frac{(n - 1)(n + 0.4319)}{n^2} \tag{12}$$

The other expression is that recently proposed by Van der Giessen et al. [1995; Equation (32)], which for $\sigma_m^\infty/\sigma_\infty > 0$ can be written as,

$$\dot{V} = \max\{\dot{V}_L, \dot{V}_H\} \tag{13a}$$

$$\frac{\dot{V}_L}{\dot{\epsilon}_\infty V} = \begin{cases} \frac{3}{2}\left\{\alpha_n\left(\frac{\sigma_m^\infty}{\sigma_\infty}\right) + \beta_n\right\}^n & \text{if } \sigma_m^\infty/\sigma_\infty \geq 1 \\ \frac{3}{2}\{\alpha_n + \beta_n\}^n \frac{\sigma_m^\infty}{\sigma_\infty} & \text{if } \sigma_m^\infty/\sigma_\infty < 1 \end{cases} \tag{13b}$$

$$\frac{\dot{V}_H}{\dot{\epsilon}_\infty V} = \begin{cases} \frac{3}{2}\left\{\frac{1}{1 - (0.87a/b)^{3/n}}\left[\alpha_n\left(\frac{\sigma_m^\infty}{\sigma_\infty}\right) + \frac{1}{n}\right]\right\}^n & \text{if } \sigma_m^\infty/\sigma_\infty \geq 1 \\ \frac{3}{2}\left\{\frac{1}{1 - (0.87a/b)^{3/n}}\left[\alpha_n + \frac{1}{n}\right]\right\}^n \frac{\sigma_m^\infty}{\sigma_\infty} & \text{if } \sigma_m^\infty/\sigma_\infty < 1 \end{cases} \tag{13c}$$

with α_n and β_n given by Equation (12). This is a refinement of the Budiansky et al. (1982) expression in two directions. Firstly, Equation (13b) includes a

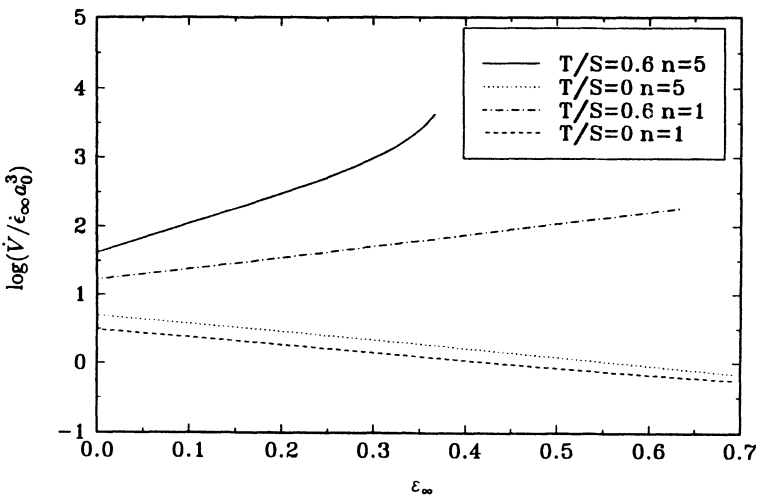

Figure 9. *Comparison of curves of normalized void growth rate versus remote strain for linear and nonlinear creeping solids at two remote stress triaxialities with* $a_0/b_0 = 0.1$.

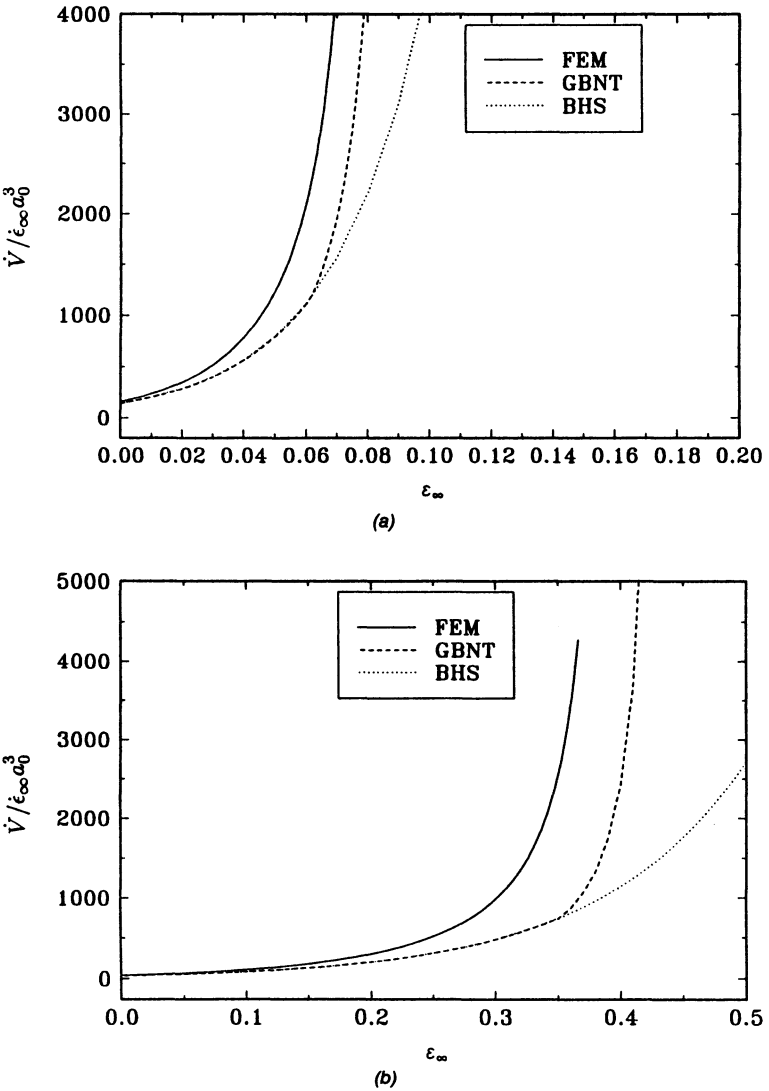

Figure 10. *Comparison of numerically computed void growth rates (FEM) with two approximate expressions for spherical voids, Budiansky, Hutchinson and Slutsky (1982) (BHS) and Van der Giessen et al. (1995) (GBNT). (a)* T/S = *0.75; (b)* T/S = *0.6; (c)* T/S = *0.*

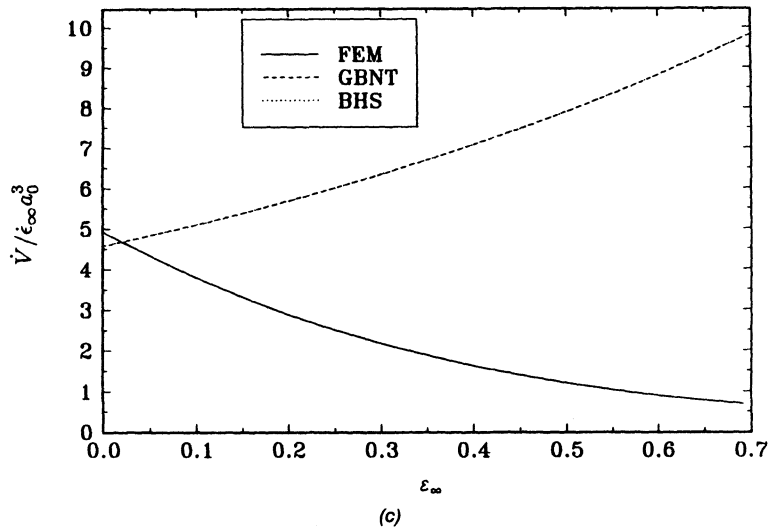

Figure 10 (continued). *Comparison of numerically computed void growth rates (FEM) with two approximate expressions for spherical voids, Budiansky, Hutchinson and Slutsky (1982) (BHS) and Van der Giessen et al. (1995) (GBNT). (a)* T/S = *0.75; (b)* T/S = *0.6; (c)* T/S = *0.*

linearization of Equation (11) proposed by Tvergaard (1984) for triaxialities $\sigma_m^\infty/\sigma_\infty < 1$. Secondly, Equation (13c) comprises a novel, high triaxiality growth rate expression for a void in an infinitely long cylinder, thus accounting in an approximate manner for void interaction; a linearized version of which is included for $\sigma_m^\infty/\sigma_\infty < 1$.

The void volume growth rates are computed by integrating Equations (11) and (13) assuming that the void remains spherical. Figure 10 compares the void volume growth rates so obtained with the cell model values. In Figure 10(a), $T/S = 0.75$; in Figure 10(b), $T/S = 0.6$; and in Figure 10(c), $T/S = 0$. The curves denoted by FEM are repeated from Figure 4, but since different scales are employed in Figures 10(a), 10(b) and 10(c), a linear rather than log plot is used. The void volume growth rates computed from Equations (11) and (13) are denoted by BHS and GBNT, respectively. With $T/S = 0.75$ and $T/S = 0.6$, the approximate formula of Van der Giessen et al. (1995) does a reasonable job of estimating the void growth history, although the void growth rates are somewhat underestimated. The approximate formula of Budiansky et al. (1982) gives identical predictions for small strains, but does not pick up the acceleration of the growth rate at larger strains. In Figure 10(c), where $T/S = 0$, the approximate formulas essentially coincide, and although both provide a good estimate of the initial growth rate, they give an entirely wrong trend for the evolution of the void growth rate. Evidently, the decrease in void growth rate arises because of the void shape

change and any approximate formula which does not account for void shape changes will not predict the correct trend.

CONCLUSIONS

Eshelby (1957) showed that an isolated void growing in an infinite, linearly viscous solid subject to remote axisymmetric stressing will always have a spheroidal shape. A similar conclusion cannot be drawn for nonlinear creeping solids. Especially in cases of non-dilute concentrations of voids, where void-void interaction is important, void growth into non-spheroidal shapes may be expected. The present model problem accounts for these aspects. However, the results obtained here indicate that for the triaxialities and creep exponents considered, and over the strain interval analyzed, the deviation from a spheroidal shape is rather small until significant necking down between voids occurs.

Budiansky and Hutchinson (1980) studied the possibility of voids growing in a self-similar shape in an infinite creeping solid. They showed that an initially spherical void instantaneously grows in a prolate spheroidal shape for all $n > 1$, except for a regime of relatively high stress triaxialities where there is a tendency to grow in an oblate fashion (see also Budiansky et al., 1982). The remote triaxialities considered here, were chosen to verify these trends for non-dilute void concentrations. The value of $T/S = 0.6$ is the triaxiality at which Budiansky and Hutchinson predict nearly self-similar growth for $n = 5$, while $T/S = 0.75$ should give the strongest tendency for growth into an oblate shape. The present finite strain growth simulations (Figure 3) confirm these trends for the initial growth. However, void interaction effects become significant after some growth [see Figures 4(b), 6 and 7], and the necking down between voids promotes an oblate shape even if the initial tendency is for a prolate shape.

The formula (11) due to Budiansky et al. (1982) has been widely used to evaluate the contribution to the growth rate of a grain boundary cavity due to creep (e.g., Sham and Needleman, 1983; Tvergaard, 1984; Van der Giessen and Tvergaard, 1994). The shape of the cavity is commonly assumed to remain the same during the deformation process. The results in Figure 10 show that the Equation (11) captures the growth rate of the initial void (with $a_0/b_0 = 0.1$) rather well, but that after substantial growth of the void, shape effects cause the agreement to deteriorate. The modification of Equation (11) contained in the formula (13) improves the agreement for moderate to high triaxialities ($T/S = 0.6$ and 0.75), as it attempts to incorporate void interaction (Van der Giessen et al., 1995). The rapidly accelerating growth rates are still underestimated significantly, but it should be noted that the growth rates are then so high that coalescence takes place within a relatively short period of time and the error in the total time to coalescence can remain modest. For low triaxialities, such as remote uniaxial tension, shape changes become even more important, and there is certainly room

for improvement in the growth rate formulas presently available. On the other hand, it should be noted that diffusive transport of matter also contributes to the growth of grain boundary cavities at elevated temperatures, and that surface diffusion along the void surface will tend to maintain a spherical or spherical-caps shape. This further complicates the void growth issues, but is outside the scope of the present work.

ACKNOWLEDGEMENTS

A. N. acknowledges the support of the Materials Research Group on *Micromechanics of Failure-Resistant Materials* at Brown University (NSF Grant DMR-9223683). We are also pleased to acknowledge use of the workstation clusters at the Pittsburgh Supercomputer Center.

REFERENCES

1. Budiansky, B. and J. W. Hutchinson. 1980. In *Proc. XVth International Congress of Theoretical and Applied Mechanics*, F. P. J. Rimrott and B. Tabarrok, eds., Amsterdam: North-Holland, p. 243.
2. Budiansky, B., J. W. Hutchinson and S. Slutsky. 1982. In *Mechanics of Solids*, H. G. Hopkins and M. J. Sewell, eds., Oxford: Pergamon Press, p. 13.
3. Eshelby, J. D. 1957. *Proc. R. Soc. Lond.*, A241:376–391.
4. Hill, R. 1956. *J. Mech. Phys. Solids*, 5:66–74.
5. Kachanov, L. M. 1986. *Introduction to Continuum Damage Mechanics*. Dordrecht, The Netherlands: Martinus Nijhoff.
6. Koplik, J. and A. Needleman. 1988. *Int. J. Solids Struct.*, 24:835–853.
7. Lee, B. J. and M. E. Mear. 1994. *ASME J. Eng. Mater. Technol.*, 116:348–358.
8. Needleman, A., V. Tvergaard and J. W. Hutchinson. 1992. *Topics in Fracture and Fatigue*, A. S. Argon, ed., New York: Springer-Verlag, p. 145.
9. Needleman, A. and J. R. Rice. 1980. *Acta Metall.*, 28:1315–1332.
10. Needleman, A. and C. F. Shih. 1978. *Comp. Meth. Appl. Mech. Eng.*, 15:223–240.
11. Sham, T. -L. and A. Needleman. 1983. *Acta Metall.*, 31:919–926.
12. Tvergaard, V. 1982. *Int. J. Fract.*, 18:237–252.
13. Tvergaard, V. 1984. *J. Mech. Phys. Solids*, 32:373–393.
14. Tvergaard, V. 1990. *Adv. Appl. Mech.*, 27:83–151.
15. Van der Giessen, E. and V. Tvergaard. 1994. *Acta Metall. Mater.*, 42:959–973.
16. Van der Giessen, E., M. W. D. Van der Burg, A. Needleman and V. Tvergaard. 1995. *J. Mech. Phys. Solids*, 43:123–165.